Synaptic vesicles in rat hippocampal boutons recycle to different pools in a use-dependent fashion

Pieter Vanden Berghe and Jürgen Klingauf

Department of Membrane Biophysics, Max-Planck Institute for Biophysical Chemistry, D-37077, Göttingen, Germany

Efficient vesicle membrane recycling at presynaptic terminals is pivotal for preventing depletion and maintaining high firing rates in neuronal networks. We used a new approach, based on the combination of spectrally different optical probes, to investigate how stimulation determines the fate of synaptic vesicles after endocytosis. We found that in the small central synapses of rat hippocampal neurones low frequency stimulation (40 action potentials at 2 Hz) targets vesicles preferentially to vesicle pools that were kinetically faster. Vesicles taken up during endocytosis triggered by high frequency stimulation (400 action potentials, 20 Hz) were also placed in the back of the release queue. We performed a spatial analysis of the recycled vesicles in living hippocampal boutons using two spectrally different FM-dyes (FM1-43 and FM5-95). By using these consecutively, vesicles endocytosed by either stimulation protocol were labelled with a different colour. This revealed that the kinetic arrangement was also reflected in the spatial organization of vesicles within the bouton. Next, we identified the postsynaptic site of the active zone by transfecting the neurones with postsynaptic density protein PSD-95-CFP. The data from these triple colour experiments suggest that retrieval after low frequency stimulation keeps vesicles in a more confined region closer to the active zone as identified by PSD-95-CFP expression at the postsynaptic site.

(Received 27 October 2005; accepted after revision 19 January 2006; first published online 26 January 2006)
Corresponding author J. Klingauf: Department of Membrane Biophysics, Max-Planck Institute for Biophysical Chemistry, D-37077, Göttingen, Germany. Email: j.klingauf@mpi-bpc.mpg.de

Accurate and fast synaptic transmission depends on efficient vesicle recycling. Several modes of membrane retrieval have been described to supply fusion-competent vesicles during ongoing stimulation. Two originally quite opposing hypotheses, in which vesicles either fuse completely (Heuser & Reese, 1973) or only make brief contact with the presynaptic membrane (Ceccarelli *et al.* 1973), found sufficient support. In the first mode, vesicles are retrieved using clathrin lattices and fuse with an endosome before being re-used (τ ~40–60 s) (Miller & Heuser, 1984; Ryan *et al.* 1993). However, if this were the sole route, synapses might not be able to keep up with fast firing rates (Pyle *et al.* 2000). Mechanisms making vesicles re-available faster ($\tau \leq 10$ s) may not require intermediate endosomal sorting (Murthy & Stevens, 1998) like in 'kiss-and-run or stay' pathways (Fesce *et al.* 1994; Klingauf *et al.* 1998; Pyle *et al.* 2000; Sun *et al.* 2002; Aravanis *et al.* 2003; Gandhi & Stevens, 2003; reviewed by Royle & Lagnado, 2003). In frog and Drosophila neuromuscular junctions (NMJ) and rat calyx of Held coexistence of different endocytic routes has been suggested (Koenig & Ikeda, 1996; Kuromi & Kidokoro, 1998, 1999, 2002; Richards *et al.* 2000, 2003; de Lange *et al.* 2003) and Kuromi & Kidokoro (2002) attribute distinct vesicle sorting within Drosophila NMJ to different endocytic routes and Ca^{2+} sources. However, Lin *et al.* (2005) could not find any evidence for the different endocytic routes in snake motor nerve terminals. At small central synapses, e.g. hippocampus, the existence of different modes remains a matter of ongoing debate (Aravanis *et al.* 2003; Gandhi & Stevens, 2003; Fernandez-Alfonso & Ryan, 2004). Vesicles in presynaptic boutons are categorized into different pools depending on release kinetics (Pieribone *et al.* 1995). Exo-endocytic cycling recruits only a fraction of available vesicles (Harata *et al.* 2001), the so-called recycling pool (RP) which typically contains ~30–45 vesicles. Part of it, the readily releasable pool (RRP), comprises vesicles (~5–10) available for immediate release at stimulus onset, increase in local $[Ca^{2+}]_i$ (Schneggenburger & Neher, 2000) or by a hypertonic pulse (Stevens & Tsujimoto, 1995; Rosenmund & Stevens, 1996). A study by Rizzoli & Betz (2004) suggests that, at least in frog NMJ, RRP vesicles are randomly distributed. However, using electron microscopy (EM) Schikorski & Stevens (2001) showed correlation between RRP vesicles and those morphologically docked at the active zone of cultured

 DOI: 10.1113/jphysiol.2005.100842

hippocampal neurones. Other recycling vesicles (reserve pool) have lower release probability and resting pool vesicles are not recruited during a set stimulation period (Sudhof, 2000). It is unclear how these pools are supplied with freshly endocytosed vesicles and whether exocytotic activity of different duration and frequency triggers selective endocytic or postendocytic routes, eventually leading to different vesicle sorting in hippocampal boutons. In view of the recent findings of Rizzoli & Betz (2004), showing that frog NMJ vesicles are not necessarily arranged in physically logic release queues, it is interesting to check whether a similar random organization was maintained. Therefore, in this study, we used spectrally different FM dyes (Betz & Bewick, 1992) and genetically encoded fluorescent proteins to investigate the fate and organization of synaptic vesicles after endocytic retrieval in fast central synapses of rat hippocampus.

Methods

Cell cultures and transfection

Hippocampal neuronal cultures were prepared from newborn rats as previously described (Klingauf *et al.* 1998). In short, newborn rats were killed by decapitation in accordance with the guidelines of the State of Lower Saxony, hippocampi were removed from the brain in ice-cold Hank's salt solution, and after 'unrolling' the dentate gyrus was cut away. After digestion with trypsin (5 mg ml^{-1}) cells were triturated mechanically and plated in MEM medium, supplemented with 10% fetal calf serum and 2% B27 supplement (all from Invitrogen GmbH, Karlsruhe, Germany). All experiments were performed between 13 and 17 days *in vitro* (DIV). The calcium phosphate method was used to transfect neurones on DIV 4 with PSD-95-eXFP in a pxCMV-vector (R. Toonen, Amsterdam). Transfected cells were used for FM experiments 9–13 days later.

Dynamic FM1-43/5-95 imaging

Experiments were performed on an inverted microscope (Axiovert 135, Carl Zeiss) with a 63 ×, 1.2 NA water immersion objective. For FM dye loading, neurones were stimulated by eliciting APs with electrical fields (1 ms, 40 mA pulses, WPI A385 stimulator) between two parallel Pt wires (∼10 mm spacing). AP-V (50 μM) and CNQX (10 μM) were present in the external solution (mM: NaCl 150, KCl 5, $MgCl_2$ 1, $CaCl_2$ 2, glucose 10, Hepes 10, pH 7.4, ∼325 mosmol l^{-1}) to prevent recurrent network activity. Between loading and destaining an 8 min washing period was observed. All experiments were performed at room temperature. Hypertonic solutions contained 500 mM sucrose and were applied for 10 s. FM dyes (Molecular Probes) were excited at 475 nm (Polychrom II monochromator, Till Photonics, Gräfelfing, Germany), emission light was passed through on a 495 nm dichroic mirror, spectrally split over a 565 nm beam splitter (custom-made by MPI, Göttingen) and projected onto a cooled CCD camera (PCO, Sensicam, Kelheim, Germany). Figure 3*B* shows the normalized spectra of FM1-43 and FM5-95 as recorded in hippocampal boutons, together with the dichroic and bandpass filters used in the kinetic recordings. Images were recorded at 2 Hz, with an exposure time of 120 ms (Till Vision, Till Photonics, Gräfelfing, Germany). Images were analysed using Till Vision (Till Photonics) and Metamorph (Universal Imaging, CA, USA) software. Circular regions of interest (1.7 μm diameter) were drawn around stained boutons and intensity changes were computed for both channels. All further signal analysis was done using custom-written macros in Igor Pro (Wavemetrics, Lake Oswego, OR, USA). Red signals were systematically corrected for 13% bleedthrough from the green channel, since 13% of the signal measured in the green channel was present as a background in the red channel (Fig. 3*C*). All boutons were destained completely in several rounds of electrical field stimulation and a high K^+ stimulation to determine background fluorescence. Dye concentrations of FM1-43 (10 μM) and FM5-95 (15 μM) were matched for nearly identical fluorescence per vesicle. By completely destaining the boutons we determined the total amount of dye uptake. For the dual FM loading protocol this allowed us to measure as well the respective fractions of FM1-43 and FM5-95 fluorescence and therefore the contribution of low and high frequency stimulation (Fig. 4*D*). For dye uptake experiments mean, errors (S.E.M.), and statistics are based on the number of dishes analysed, thereby taking into account the dish-to-dish variation, and not on the large total number of boutons, which would cause errors to virtually vanish. The exponential fits (Igor Pro, Wavemetrics) for the destaining profiles were performed on the curves of individual boutons. The destaining constants were averaged and compared or pooled with the averages obtained from other dishes. All values were compared with ANOVA or Student's *t* test, unless mentioned otherwise. '*N*' denotes the dish numbers while '*n*' is used for the number of boutons.

Confocal microscopy

All spatial measurements were performed on high resolution images recorded with a TCS SP2 confocal unit (pinhole 1.5 airy) coupled to an inverted microscope (Leica, Mannheim, Germany). The 488 line of an Ar laser was used to excite both FM1-43 and FM5-95. The laser beam was expanded to overfill the objective (Plan Apochromat, 63 ×, 1.2 NA water immersion objective) and maximize resolution. Several (3–4) images were averaged to reduce

photon shot noise and obtain images with high signal-to-noise ratios; settings were chosen such that background and high intensity spots fell within the dynamic range of the PMTs. In order to detect differences in relative position, smaller than the diffraction-limited resolution of the confocal microscope, we labelled both objects with different colours. Dual-colour imaging by laser scanning could in principle introduce two significant error sources (besides several noise sources): chromatic aberrations of the optical system and the limited reproducibility of the scanning process. The imprecision of the scanner (typically about 20–30 nm for the magnification of the objective and the beam path length used here) was not an issue here, since we recorded both colour channels simultaneously by excitation of both fluorophores with the very same laser line (488 nm). We then checked for chromatic aberration of the optics by measurements of orange 40 nm beads which were also excited by the 488 nm laser line and could be detected in both the green and red channels (same settings as for FM dyes). In this way we determined the resolution of our system for relative position measurements to be ~25 nm (cf. Fig. 6*F* and *G*). Given this resolution we could not detect any significant chromatic aberration in the central part of the field of view that was used for FM measurements in living synaptic boutons. Dual colour images were recorded simultaneously with detection slits of 550/60 nm and 690/60 nm for FM1-43 and FM5-95, respectively. Simultaneous recording of two dyes, excited with the same laser beam, rendered this procedure insensitive also to error sources like bouton shift and stage drift. Images were over-sampled (pixel size of 20–60 nm) to facilitate the Gaussian fitting routines.

Spatial analysis

Within rectangular regions of interest, 2-D Gaussian curves were fitted using custom-written routines (Igor Pro). A first 2-D Gaussian fit determined width in the x and y direction and a correlation factor which was fed into a second fitting step, returning the widths (at e^{-1}) of the fluorescent spot along its major and minor axes and also the centre (or centres for dual colour) of the boutons. Several controls were performed to assure that the spatial differences were not due to technical issues. First we screened for correlation of the displacement with signal intensity (in the red and green channel), noise levels and position within the image, the latter to avoid any involvement of spherical or spatial aberration. No dependency with any of these parameters was observed. The precision (~25 nm) of scanning and fitting procedures for dual colour experiments was assessed using either 40 nm orange fluorescent beads (Molecular Probes) or a mixture of FM1-43 and FM5-95 to determine precision (~40 nm) within living boutons. These measurements assess the magnitude of aberrations or differences in focus intrinsic to the microscope optics and the biological specimen. Differences in position of the two colours allowed us to calculate relative distances as well as position vectors (e.g. from red to green). We define α to be the angle of the position vector (with the frame of the image) (Fig. 7*A*) and, assuming a bouton makes synaptic contact directly with the postsynaptic site facing it, then β is defined to be the angle of the normal to the post-synaptic surface (as determined based on the information in the differential interference contrast (DIC) image 1, see Fig. 7*A*). The angles α and β were determined independently for each bouton. As a control, angles α were compared with randomized angles β. Cells transfected with PSD-95-CFP were imaged using the 458 nm line of the Ar laser and a detection slit of 490/50 nm. All spatial measurements were compared with Student's t test, unless mentioned otherwise.

Simulation

We considered a three pool and one membrane compartment model to describe the destaining of FM dyes (Fig. 5*C*). Pool p1 represents the RRP, p2 the RP, and p3 the resting pool that is hardly mobilized during a 400 AP (20 Hz, 20 s) stimulus. From p1, vesicles release FM dyes into the membrane dye pool m, from where they slowly departition into the external solution to become non-fluorescent. This last step is the actual observable. Transition rates $k_{n+1,n}$ for this exemplary model were chosen based on published data and own earlier experimental findings. For k_{32} we used a time constant of 180 s, slow enough to mimic the negligible forward mixing (Figs 2*B* and 4*E*); $k_{21} = 0.2\ s^{-1}$ reflects the refilling time constant of the RRP (Stevens & Tsujimoto, 1995); $k_{rel} = 1\ s^{-1}$ implies that the RRP will be depleted by 87% after 2 s, i.e. after 40 APs, the stimulus reported to release most RRP vesicles in hippocampal boutons (Murthy & Stevens, 1999); and $k_d = 0.2\ s^{-1}$ is the measured departitioning rate, which reflects the clearance of both dyes out of the synaptic cleft, which may involve repeated partitioning and departitioning (Klingauf *et al.* 1998). Recycling was not considered, since we are focusing on the acute use (destaining) of the pools starting from a steady state reached during the wash-out period. Destaining under prolonged stimulation may be affected

Image 1

by rapid re-use (Pyle *et al.* 2000), but FM dye pulse chase experiments under continued stimulation gave no indication of significant re-use during the first seconds (V. J. Mueller & J. Klingauf, unpublished results) in line with a recent study by Li *et al.* (2005) in hippocampal cultures derived from transgenic pHluorin mice. Numeric solutions for the differential equations were computed using Runge-Kutta iterations provided by Igor Pro macro language (Wavemetrics).

Results

Biphasic membrane retrieval during strong stimulation

First we investigated whether different endocytic routes are triggered by exocytic events of different frequency. Cultured hippocampal neurones were stimulated in the presence of 10 μM FM1-43 for a set number of action potentials (APs) either at 2 or 20 Hz (Fig. 1*A* and *B*). The cells received a finite number of APs lasting maximally 20 s (1–40 AP at 2 Hz or 1–400 AP at 20 Hz) (Fig. 1*A*). The total exposure to FM1-43 was 35 s, short enough to limit unspecific staining but long enough to allow endocytosis to take place at least for 10 s after the longest stimulation. The boutons were completely destained by two trains of 400 AP (20 Hz) and a consecutive application of high K^+ (Fig. 1*C*) and the total fluorescence loss was determined. Most coverslips ($N = 36$) were exposed twice to this procedure so that a total of 72 datapoints were obtained for the 18 conditions studied. This loss reflects the number of previously endocytosed vesicles and can be expressed (± S.E.M.) as function of stimulus duration or number of APs used to stain the boutons initially (Fig. 1*D* and *E*). The curve representing the 2 Hz stimuli (triangles) is well fitted by a single exponential. Similarly, during the first 80–100 APs the 20 Hz stimulus curve (circles) behaves mono-exponentially, while for prolonged stimulation dye uptake displayed a biphasic time course. About 4–5 s after stimulus onset, a second phase of membrane uptake retrieves the next contingent of fluorescent vesicles different from those used during the first 80 APs (Fig. 1*D*). Alternatively, complete

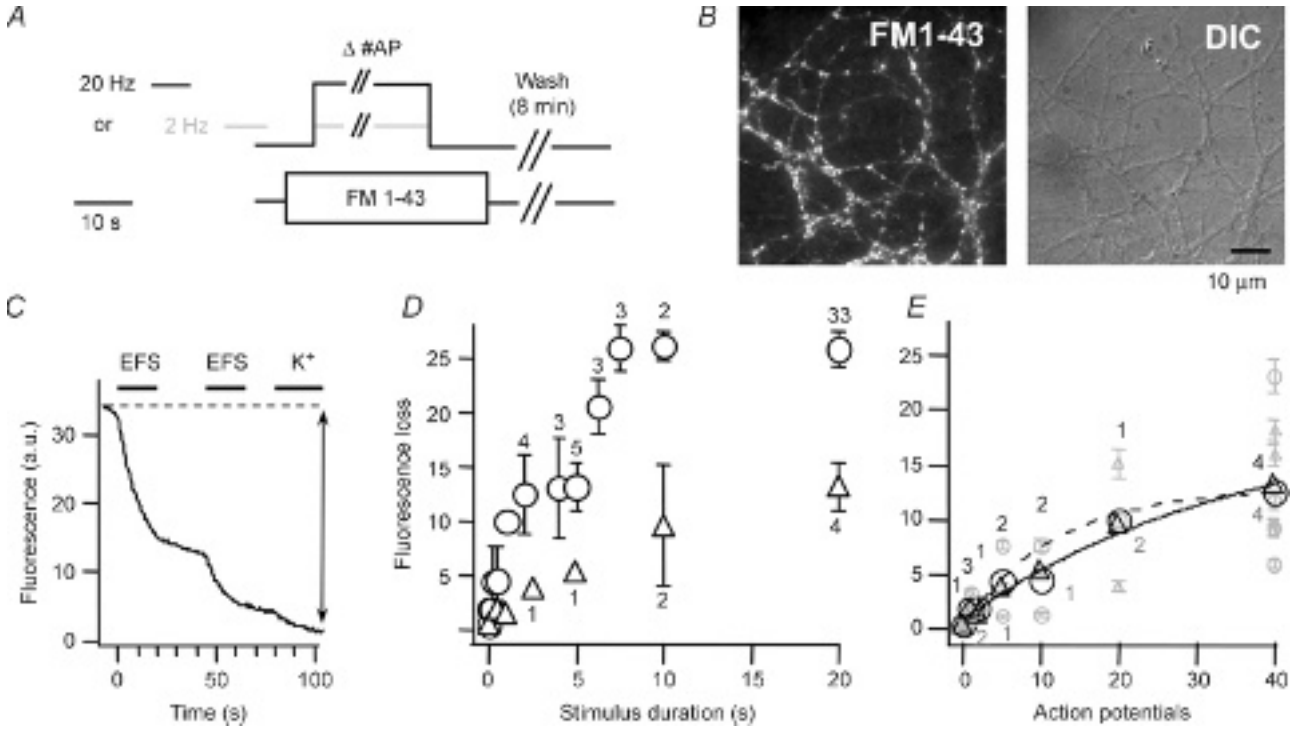

Figure 1. Stimulus-dependent fluorescence upload and destaining
A, action potentials (APs) were elicited by electric field stimulation (EFS) either at 2 (grey) or 20 Hz (black) to stain hippocampal boutons with FM1-43 (10 μM, 35 s). Different coverslips ($N = 36$) received a set number of APs ranging from 1 to 40 (2 Hz) and 1–400 (20 Hz) such that delayed endocytosis could occur for at least 10 s. *B*, representative FM1-43 and differential interference contrast images. *C*, all boutons were completely destained by 3 consecutive stimuli; 2 rounds of electrical field stimulation (EFS) and a high K^+ application (indicated by bars). *D* and *E*, total fluorescence loss, reflecting the number of endocytosed vesicles plotted against stimulation duration (*D*) or AP numbers (*E*). Triangles and circles represent the average (± S.E.M.) loss of 2 and 20 Hz loading, respectively (figures close to symbols are the number of different coverslips). Note the plateau after 3–5 s in the 20 Hz curve. Grey symbols (*E*) are bouton averages (± S.E.M., $n > 30$) of individual coverslips.

cessation of exo- and endocytosis would also explain the plateau for stimuli of about 4–5 s. Although postsynaptic current recordings never display such a sudden halt, a quite substantial depression in exocytosis can be observed (Rosenmund & Stevens, 1996). The mechanisms underlying this characteristic upload pattern are not clear, but data from Drosophila NMJ suggest that Ca^{2+} may play an important role (Kuromi & Kidokoro, 2002; Kuromi *et al.* 2004). We conclude that at least two processes govern endocytosis during prolonged 20 Hz stimuli in hippocampal boutons. Another interesting finding was that for a small number of APs (~40) dye uptake did not differ when stimulated at 2 or 20 Hz (Fig. 1*E*), suggesting that the same vesicle number is utilized for the kinetically faster component independent of stimulation frequency.

Different upload leads to different destaining

Next we investigated whether these endocytic processes would sort vesicles differently leading to specific re-use during a next round of stimulation. It has been suggested that specific endocytotic routes cater for different pools (Pyle *et al.* 2000; Richards *et al.* 2000; Kuromi & Kidokoro, 2002). Therefore we tested whether in hippocampal boutons, vesicles retrieved by either high or low frequency stimulation were sorted back differentially into the different kinetically defined pools. Synapses were loaded with FM1-43 by either high frequency stimulation (2 × 400 APs; 20 Hz) to label most of the recycling vesicles or low frequency stimulation (2 × 40 APs; 2 Hz) which labels a different set or a fraction of the vesicles utilized during high frequency stimulation (Fig. 2*A*). The AP numbers were chosen to be on either side of the upload plateau observed in Fig. 1*D*, and assuming the same vesicles were re-used, we repeated the stimulus to maximize dye exchange. Assuming the fate of each vesicle retrieved by either loading protocol were the same, then normalized bouton destaining kinetics would have to be identical. However, the destaining during a 20 Hz (400 AP) stimulus (Fig. 2*B*) reveals that boutons stained under low frequency stimulation lose relatively more dye with faster kinetics (time to reach 50% of the first dye release ($t_{50\%}$): ~5 s) than after high frequency stimulation (circles) ($t_{50\%}$: ~8 s). This is in line with findings at the frog NMJ (Richards *et al.* 2000, 2003; Rizzoli & Betz, 2004). Therefore we conclude that vesicles uploaded after low frequency stimulation are either arranged or tagged such that they have a higher re-use probability. If the uptake and recycling refilled the bouton in a non-organized way, then drawing vesicles from a random mix of unstained and stained vesicles would lead to identical average destaining profiles after normalization (Fig. 2*C*).

Dual colour labelling of different pools in single boutons

We also developed a technique to simultaneously monitor vesicles retrieved after either low or high frequency stimulation in a single bouton. Here, instead of dyes with differing departitioning characteristics (Klingauf *et al.* 1998; Pyle *et al.* 2000; Virmani *et al.* 2003), we selected FM dyes (FM1-43 and 5-95) which were spectrally different, but had similar departitioning characteristics (Fig. 3*A*). Boutons were stimulated strongly (2 × 400 APs; 20 Hz) in the presence of one dye and, after wash-out, stimulated again (2 × 40 APs; 2 Hz) with the second dye present (Fig. 4*A*–*C*). Dye concentrations were chosen

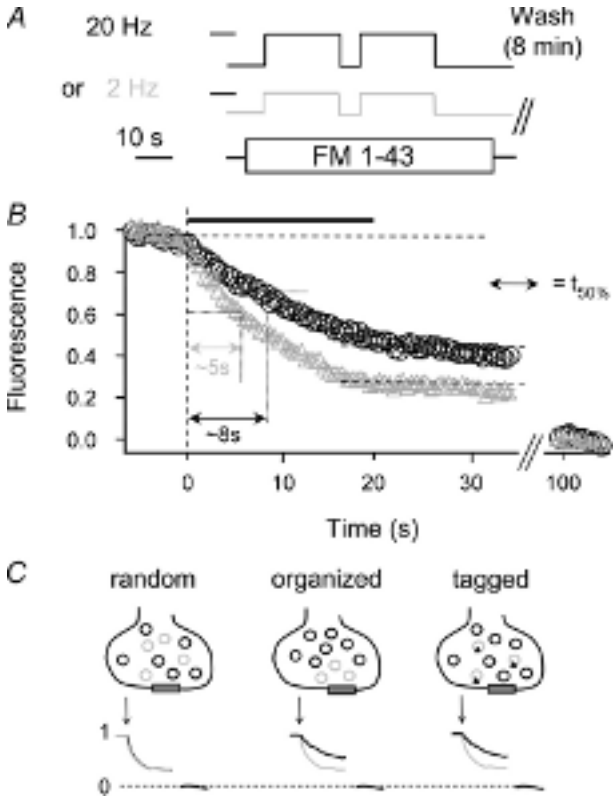

Figure 2. Bouton destaining after low or high frequency stimulus loading
A, boutons were stained with two rounds of either 400 APs (20 Hz, black) or 40 APs (2 Hz, grey) during 70 s FM1-43 exposure. *B*, normalized destaining profiles of boutons (loaded as in *A*) during a 20 Hz stimulus (black bar). The graphs show that boutons stained under low frequency stimulation lose a larger fraction of dye during a 400 AP (20 Hz) stimulus. The time to reach 50% of the first destaining step ($t_{50\%}$) was calculated as indicated. The $t_{50\%}$ values reveal that boutons stained under low frequency stimulation also destain faster (grey triangles, $t_{50\%}$ = ~5 s) than after loading with high frequency stimulation (black circles, $t_{50\%}$ = ~8 s). *C*, schematic illustrating that differences in normalized destaining (1, before; and 0, after complete destaining) can occur only if the vesicles from 2 different loading protocols (black and grey) are specifically organized or tagged. If vesicles were distributed randomly, their normalized destaining profiles would be identical.

to yield similar fluorescence per vesicle, as determined in preliminary experiments (data not shown). Boutons were always completely destained which allowed us to determine the total amount of fluorescence that was taken up. Since the two FM dyes were matched to generate similar counts per vesicle, the fraction of FM1-43 (green) and FM5-95 (red) was basically a measure for the fraction of vesicles stained with either low or high frequency stimulation (∼30% and ∼70%, respectively; $n = 241$ boutons) (Fig. 4*D*). The destaining curves again show that vesicles taken up after low frequency stimulation are organized or tagged such that they are re-used preferentially (Fig. 4*E*). This can also be seen from the ratio of destaining curves (high over low frequency loading) as it ramps up during destaining, indicating preferential use of the latter vesicles (Fig. 4*F*). Similarly, the $t_{50\%}$ (see Fig. 2*B*) is significantly smaller ($P = 0.01$, $N = 3$, $n = 81$) for low ($t_{50\%}$: 7.4 ± 0.2 s) than for high frequency stimulation ($t_{50\%}$: 8.5 ± 0.2 s), but independent of the dyes used (Fig. 4*E* and *G*). Furthermore, 400 APs (20 Hz) released a larger fraction from the low than from the high frequency stimulation vesicles (∼70% *versus* 64%) ($N = 3$, $n = 81$). To investigate whether an even stronger stimulus would enhance the differential sorting, we used

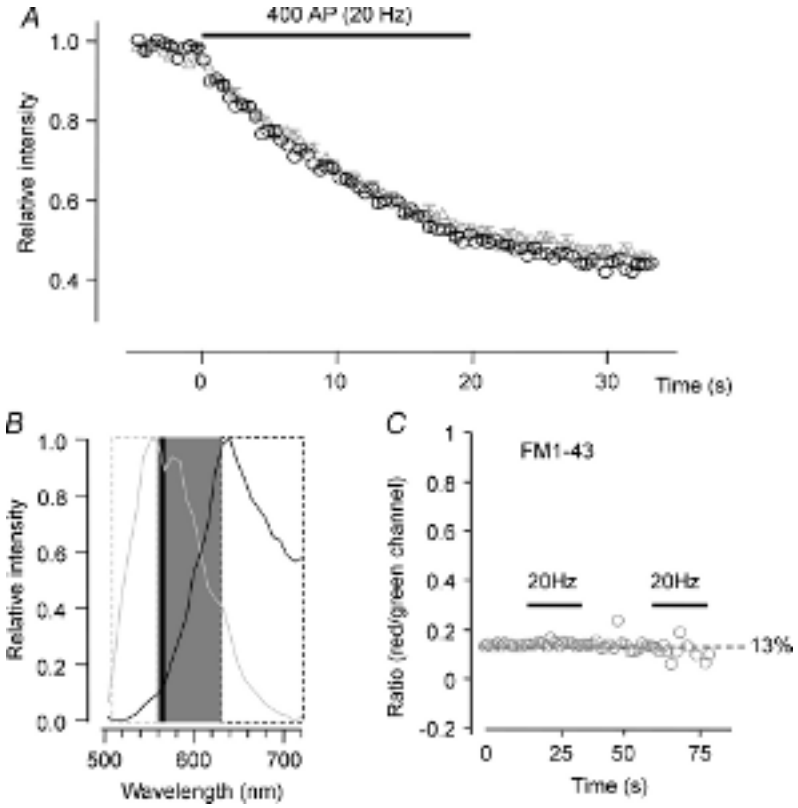

Figure 3. Technical aspects of dual staining/destaining with FM1-43/FM5-95
A, destaining of FM1-43 and FM5-95 boutons. In preliminary experiments, concentrations of both FM dyes were adjusted to match fluorescence intensity on the CCD chip; 10 μM for FM1-43 and 15 μM for FM5-95 were therefore used throughout the study. Destaining of boutons with the same number of action potentials (here: 2 × 400 APs; FM1-43, grey triangles: FM5-95, black circles) was similar during a 20 Hz destaining stimulus ($t_{50\%}$ and remaining fractions of FM1-43 or FM5-95 were not different, $n = 24$, N.S.). This indicates that the dyes are similar enough with respect to departitioning time constants to be used interchangeably. *B*, spectra of FM1-43 (grey) and FM5-95 (black) in living boutons. Hippocampal boutons were stained with electrical field stimulation in the presence of either FM1-43 or FM5-95. A spectral scan (40 points equally spaced over a range of 500–720 nm) was performed with a Leica TCS SP2 confocal microscope and spectra were normalized. In kinetic experiments, emission signals were spectrally split with a 565 dichroic mirror (black vertical line). The shorter and longer wavelength light passed through a 535/50 nm bandpass (grey dashed box) and a 630 long pass filter (black dashed box), respectively; emission light in the shaded box was not used. Images were then projected next to each other onto the chip of a CCD camera. *C*, boutons loaded with either colour were destained and bleed-through was determined as the ratio between fluorescence intensity in the 'false' over the 'correct' channel. FM5-95 could not be measured in the green channel, while the contribution of FM1-43 to the red channel was ∼13% of the signal measured in the green channel. Bleed-through was determined during destaining and found to be constant for decreasing intensities.

high K^+ as the primary stimulus followed by 2 × 40 AP with the other FM dye ($N = 3$, $n = 184$). Here again, a 20 s (20 Hz) stimulus released more dye (> 70%) from the low frequency loading than from the high K^+ loading. From the latter only 60% was released, which was more extreme than in the case of two electrical stimulus trains (Fig. 5*A*). We also probed dual coloured boutons with stimuli, known to release the RRP: a hyperosmotic sucrose pulse (Rosenmund & Stevens, 1996) and a limited number of APs (here 70). Each drew a larger fraction from low than from high frequency stimulation vesicles (Fig. 5*B*). Thus the RRP contains a larger fraction (about two times)

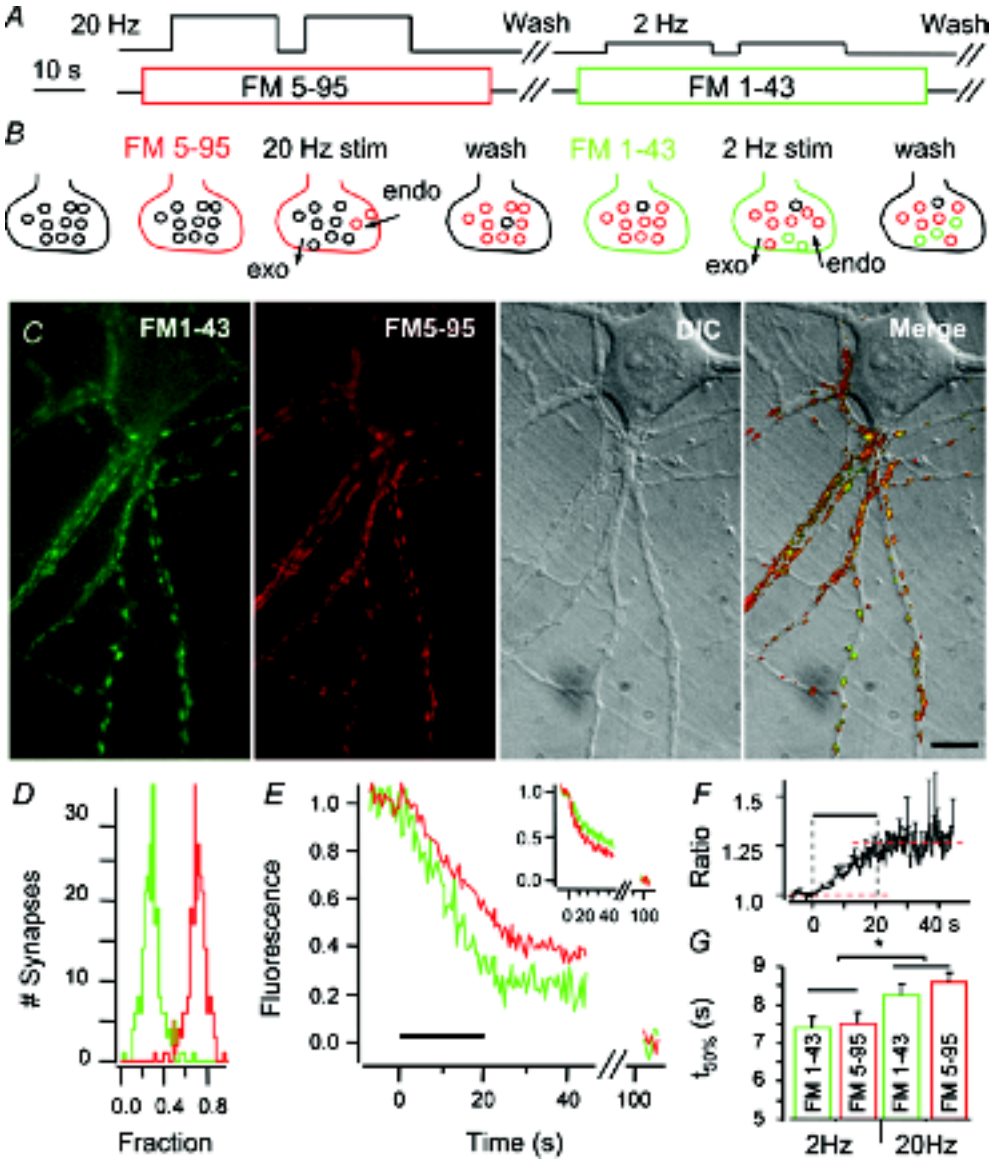

Figure 4. Dual colour labelling of hippocampal boutons
A and *B*, hippocampal neurones were stimulated with 2 × 400 APs at 20 Hz (high frequency) in 15 μM FM5-95 and after wash-out, stimulated again with 2 × 40 APs at 2 Hz (low frequency) in 10 μM FM1-43. *C*, exemplar pictures of boutons with both green (FM1-43) and red (FM5-95) vesicles. The 2 right panels show DIC and merged images of same field of view (bar = 10 μm). *D*, fraction histogram of high frequency (red) and low frequency (green) stimulation fluorescence per bouton after complete destaining. *E*, normalized high (red) and low frequency (green) stimulation signals in one bouton follow different time courses during destaining (20 Hz, 20 s). Inset: the same result is obtained when colours are swapped, that is FM1-43 (green) during high and FM5-95 (red) during the low frequency stimulus. *F*, the ratio of destaining profiles (high over low frequency loading) ramps up during destaining, indicating that vesicles loaded with the latter stimulus are used preferentially. *G*, the destaining $t_{50\%}$ for low and high frequency stimulation loading was significantly different ($^*P < 0.02$), independent of the dye. Error bars in *F* and *G* are S.E.M. of 3 different coverslips.

of vesicles loaded with low frequency stimulation. We used a numerical model assuming three sequential release pools and one membrane compartment (see Methods, Fig. 5*C*) to illustrate the observations that disparate destaining occurs if vesicles of different colour are not homogeneously distributed over the pools: a larger fraction of low frequency stimulation vesicles must sit in front and a smaller fraction in the back of the release queue. Figure 5*D* shows the fractions of dye that are released after stepwise destaining. The signals were normalized before destaining and again after 70 AP. The differences in fractions reveal that early on during destaining dyes are not equally distributed throughout the pools recruited, whereas at the end of the destaining red and green vesicles behave kinetically the same and equal fractions of dye are set free (Fig. 5*D*).

Spatial organization of vesicle pools in live boutons

Distinct sorting over recycling and resting pools might also result in spatial segregation, provided that functional pools were organized in a release queue as shown in the scheme in Fig. 5*C*. To investigate whether this was the case, different sets of boutons were stained just with one dye (FM1-43) during low or high frequency stimulation. Both shape and position were determined by 2-D Gaussian fitting in high resolution confocal images. The apparent size of the vesicle cluster, measured at 1/e of the Gaussian fit, was significantly larger after high (0.45 μm^2, $n = 229$, from 5 images) than after low frequency stimulation (0.28 μm^2, $n = 294$, from 5 images, $P < 0.001$) (Fig. 6*A* and *B*). Moreover, we found that high frequency stimulation spots were significantly more ellipsoidal (axis ratio: 1.68 ± 0.03 *versus* 1.50 ± 0.02,

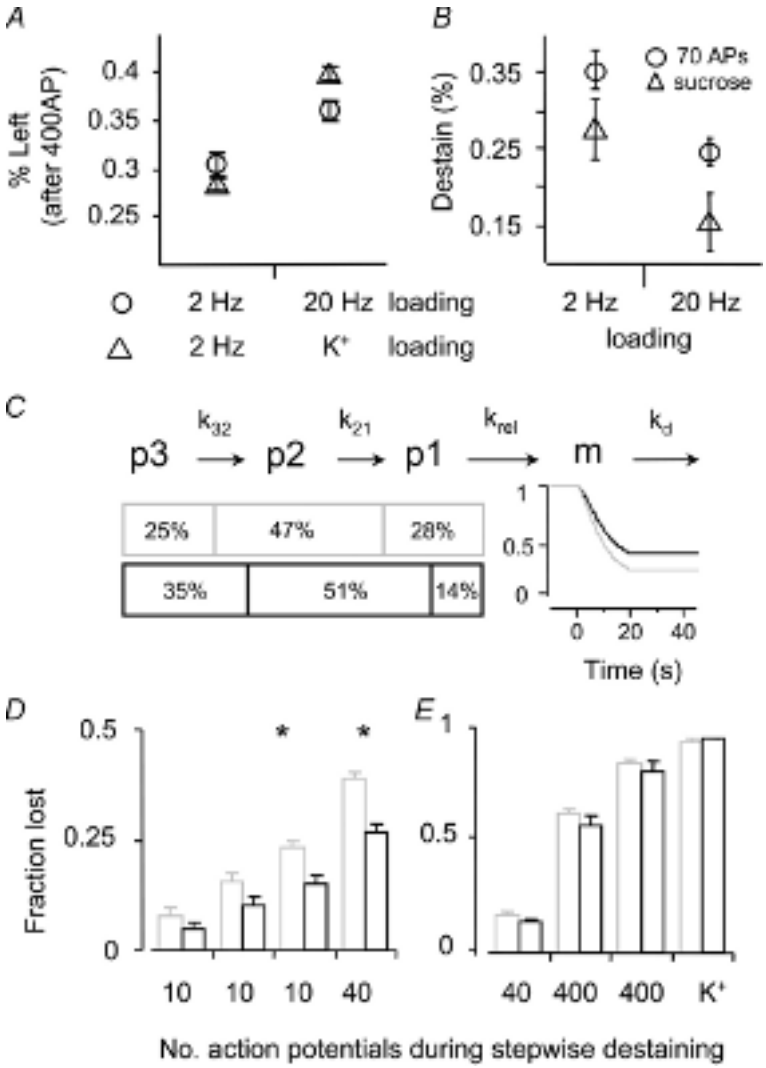

Figure 5. Differential labelling of vesicle pools
B, stimuli known to release the RRP (70 AP or a sucrose pulse) drew a larger fraction (± S.E.M., $n = 3$) of the dye loaded with low frequency stimulation. *C*, a model consisting of 3 consecutive vesicle pools (p3 = resting pool, p2 = recycling pool (RP), p1 = readily releasable pool (RRP)) with rate constants $k_{32} = 0.33$ min^{-1}, $k_{21} = 0.2$ s^{-1} and $k_{rel} = 1$ s^{-1}, and a membrane from which dye is cleared with $k_d = 0.2$ s^{-1} (cf. Methods). The model describes the measured data only if coloured vesicles are unequally distributed, with a higher percentage of low frequency stimulation (grey) vesicles in the faster pools. Percentages in p1 reflect sucrose responses (*B*) and in p3 the residual fluorescence after high frequency destaining (*A*). *D* and *E*, fractions of dye that are released after stepwise destaining. All boutons were loaded with the dual loading protocol and measured after short stimuli. In between the stimuli sufficient time was left for the dye to departition from the membrane. This is analogous to *B*, in which the release evoked by 70 APs was compared to that by a hypertonic sucrose pulse. *D*, fractions of low (grey) and high frequency (black) stimulation vesicles lost after 3 × 10 and 1 × 40 (20 Hz) action potentials (*significant differences, $P < 0.01$). *E*, signals were renormalized after the 70 first action potentials and again the fractional loss was plotted for the two colours (grey: low and black: high frequency). Further stimulation (40 APs, 2 × 400 APs and high K^+) did no longer draw different fractions from either low or high frequency stimulation vesicles. This graph shows that early on in the destaining, dyes are not equally distributed in the pools recruited (*D*), but this indicates that vesicles in the back of the release queue behave kinetically the same (randomly mixed in one pool) and equal fractions of dye are set free (*E*).

$P < 0.001$, Fig. 6*C*). Both findings are unexpected if a reasonable amount of stained vesicles were to mix freely within the terminal. Next, we used the spectrally different FM dyes to determine whether loading protocols arranged vesicles differently in a living bouton (Fig. 6*D* and *E*). Gaussian fitting used to determine the vesicle cluster centre divulged a spatial inhomogeneity (Fig. 6*F*). The radial distance between low and high frequency stimulation cluster centres was significantly larger ($n = 336$, $N = 12$, 3 of which with reverse dye protocol) in boutons after dual than after mixed dye loading (Fig. 6*G*). The difference of ~30 nm may appear small, but it is however, substantial because of the inherent problem of projecting a 3-D vesicle cluster onto a 2-D image. All spatial differences in the *z*-direction (microscope's axial direction) cannot be detected in the 2-D image and leads to an underestimation of the average displacement in our analysis and obscures putative larger differences. Moreover, labelled vesicles are distributed over all three pools (Fig. 5*C*). These findings suggest that retrieved vesicles are definitely not arranged randomly, neither kinetically nor spatially, within the hippocampal bouton.

Orientation of vesicles relative to postsynaptic structures

Finally, we wanted to investigate the orientation of vesicles relative to release sites in living hippocampal boutons. Recently, Rizzoli & Betz (2004) have shown that RRP vesicles in frog NMJ dispersed almost randomly (Rizzoli & Betz, 2004), implying a memory tag for privileged re-use. The question remains whether in fast central synapses RRP vesicles have a preferential location closer to the active zone. We consider a textbook model of a synapse (Fig. 7*A*), in which the vesicles ready to fuse sit first in line, while other vesicles are farther away and with an active zone directly opposing the postsynaptic membrane. In this model we can draw a projection vector, pointing from the

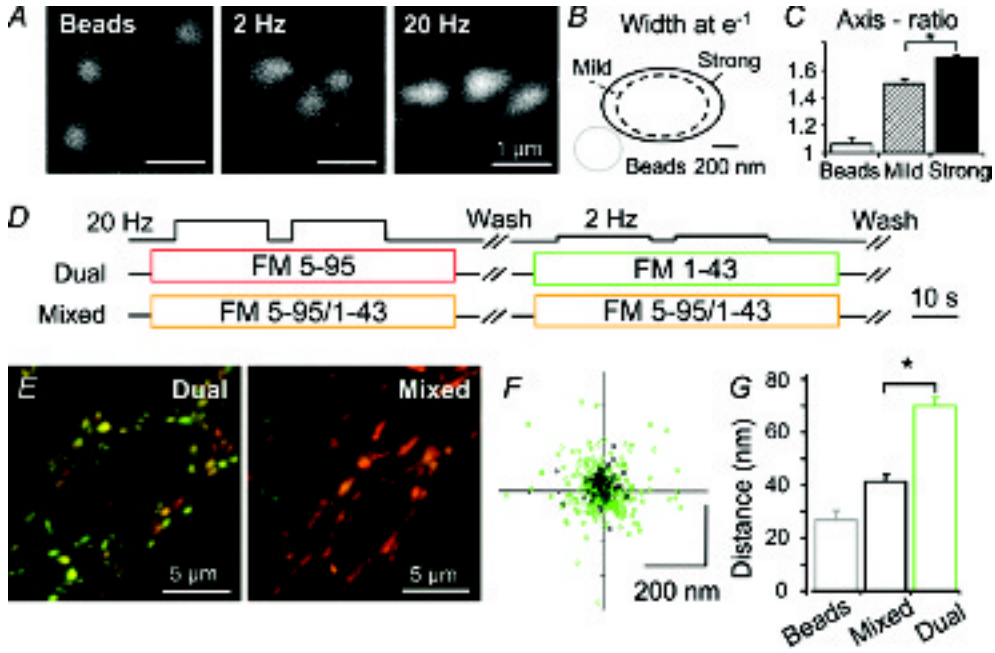

Figure 6. Spatial organization of vesicle clusters
A, fluorescent 40 nm beads, synapses loaded with FM1-43 during low frequency (2 × 40 APs, 2 Hz) and high frequency stimulation (2 × 400 APs, 20 Hz) were confocally scanned and fitted with 2-D Gaussians to determine position and shape. *B*, the apparent size (at e^{-1}) was larger for high frequency stimulation vesicle clusters (0.452 μm^2, $n = 229$; *versus* 0.286 μm^2, $n = 294$, $^*P < 0.001$). *C*, moreover shapes were more ellipsoidal: the ratio between major and minor axis was significantly higher for high frequency stimulation vesicle clusters (1.68 ± 0.03 *versus* 1.50 ± 0.02, $P < 0.001$). *D*, dual colour or mixed dye (control) protocols were used to stain boutons. *E*, merge of confocal images simultaneously taken in green and red channels. Boutons after dual staining show a slight segregation of green and red fluorescence, while those stained with mixed dyes appear uniformly orange. *x*,*y* positions (centre of intensity, COI) of red and green vesicle clusters were determined by 2-D Gaussian fits. *F*, scatter plot of low frequency COI coordinates relative to high frequency stimulation spots (the latter were always set to $(x,y) = (0,0)$). Data points from dual loading (green) are significantly more dispersed than controls (black) from mixed loading. *G*, summary of the displacement between red and green fluorescence of: orange 40 nm beads (reflecting the procedure's technical precision) and boutons stained with mixed dyes (mixed: 41 ± 3 nm; reflecting the procedure's precision in live boutons) or a consecutive application of the dyes (dual: 71 ± 3 nm) ($^*P < 0.001$).

pre-towards the postsynaptic site, with the assumption that the pre- and postsynaptic surfaces are perpendicular to the image plane (or coverslip). We also assume that the DIC and FM images, scanned simultaneously with the fluorescent bouton in focus, obey the same assumption. Projection vectors were derived based on the structural information in the DIC images (Fig. 7*B*). This vector makes an angle β with the image frame. We compared this with the vector derived from the dual colour experiments. The difference between spots loaded by either low (green) and high (red) frequency allowed us to determine a position vector (from red to green centres), which in turn makes an angle α (Fig. 7*A*) with the image frame (cf. Methods). The absolute difference angle ($|\delta_{\alpha,\beta}|$) is

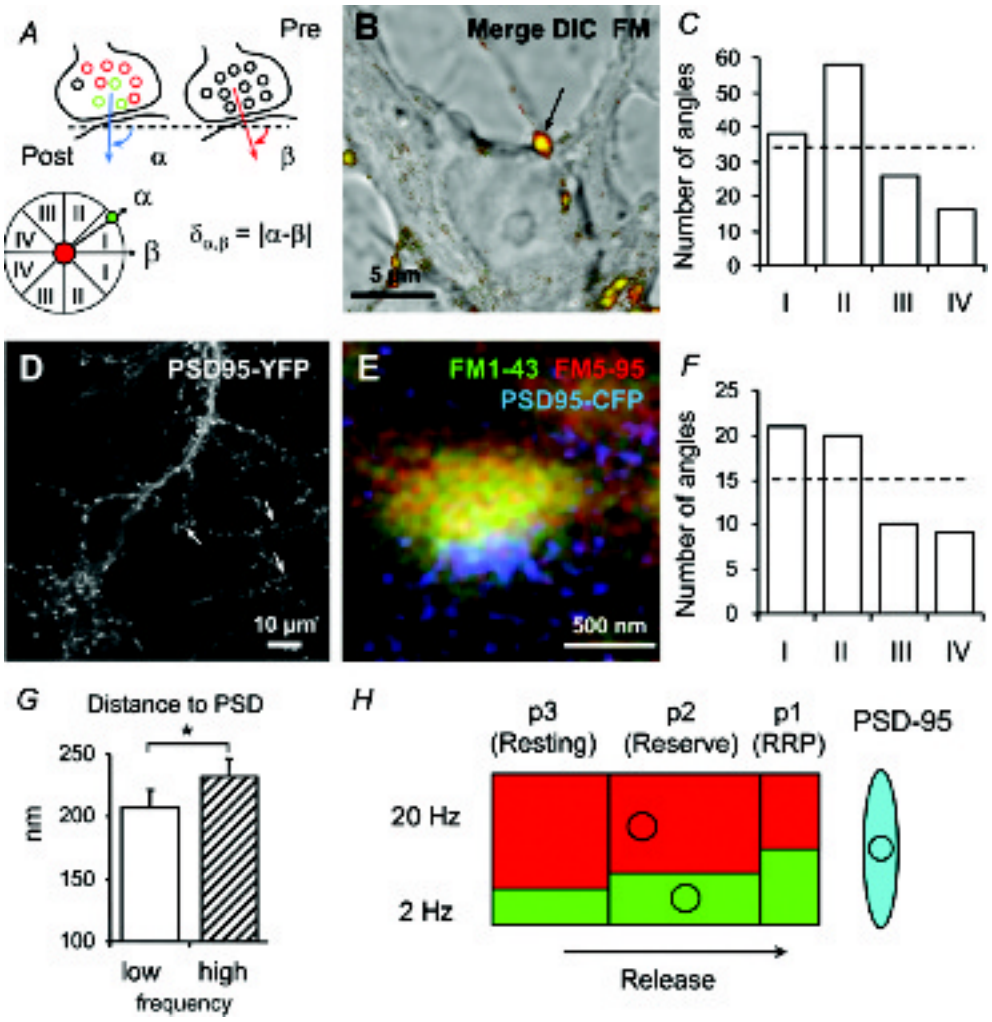

Figure 7. Orientation of vesicle clusters relative to postsynaptic sites
A and *B*, the position vector of green (low frequency) and red (high frequency) vesicle clusters makes an angle α with the image frame. Assuming a bouton (arrow) releases vesicles straight towards the postsynaptic cell, then β (angle between the normal – from the bouton to the 'postsynaptic' membrane – and the image frame) can be derived in many cases from confocal DIC images. *C*, absolute difference angles ($|\delta_{\alpha,\beta}|$) show an unequal distribution (χ^2, $P = 0.02$). Roman numbers indicate bin widths according to *A*, lower panel. *D*, hippocampal neurones transfected with PSD-95-YFP display punctate staining. *E*, exemplar confocal triple colour image of a bouton synapsing onto a PSD-95-CFP-transfected neurone after stimulation with the dual colour protocol (FM1-43: low frequency stimulation). Note the piled arrangement of high frequency (red), low frequency (green) stimulation vesicles, and PSD (blue). *F*, angle analysis again shows unequal distribution over the four bins (χ^2, $P = 0.01$), suggesting that low frequency stimulation vesicles are sorted towards the active zone. *G*, average radial distances of vesicle clusters from the PSD (208 ± 13 *versus* 232 ± 14 nm, paired *t* test, $^*P < 0.01$). *H*, a schematic summarizing kinetic and spatial characteristics of vesicles retrieved after either low or high frequency stimulation. A larger percentage of low frequency stimulation vesicles occupies the faster pools, which are located closer to the active zone (circles indicate COIs). RRP and reserve pool together constitute the recycling pool. The red and green colours, respectively, represent the vesicles labelled during high and low frequency stimulation. The arrow indicates that vesicles are released towards the active zone (PSD-95 spot).

an estimate of the model's validity, whereby a zero difference would mean that the vesicles loaded with 2 Hz are sitting closer to the active zone with the vesicles loaded with 20 Hz in the back. We found an average $\delta_{\alpha,\beta}$ of 75.6 ± 3.6 deg. The histogram of these angle differences (Fig. 7*C*) revealed a non-random distribution (χ^2, $P = 0.02$), with a preferential filling of the first and second bins. This suggests that low frequency stimulation vesicles are indeed, albeit not exactly, positioned towards the active zone. Although highly reproducible, estimation of directions based on DIC images is far from flawless. Thus, we unequivocally identified postsynaptic sites by expressing the postsynaptic density protein 95 (PSD-95) fused to a fluorescent protein in hippocampal neurones (Fig. 7*D*). The punctate appearance indicates that the mutant protein has been correctly sorted into the postsynaptic compartments (arrows). We used a cyan variant (PSD-95-CFP) in combination with dual FM loading to obtain triple colour images (Fig. 7*E*). The projection angles were analysed as above, but now postsynaptic sites were identified by fitting PSD-95-CFP spots. Again the histogram showed an uneven angle distribution (χ^2, $P = 0.01$) (Fig. 7*F*) with the average angle (72.3 ± 6.6 deg) not different from the estimate using DIC images. Accordingly we found that the radial distance to the postsynaptic site was smaller for low frequency stimulation vesicles (232 ± 14 nm *versus* 208 ± 13 nm, $P < 0.01$, paired *t* test, $n = 60$) (Fig. 7*G*). Since these vesicles also preferentially populate kinetically faster pools (Fig. 5*C*), it suggests that the latter are positioned closer to the active zone.

Discussion

Our study provides evidence for a differential kinetic sorting of synaptic vesicles in hippocampal boutons depending on the stimulus frequency. We designed a method based on spectrally different probes to label vesicles endocytosed by either high or low frequency stimulation and found that the latter are privileged in terms of re-use. While endocytosis triggered by high frequency stimulation fills up the whole release queue, milder stimuli favoured vesicle re-use, generating a shortcut to the front of the release queue. We also found that in hippocampal boutons the ready-to-fuse vesicles seemed to be orientated towards the active zone as became clear from triple colour (FM1-43, FM5-95, PSD-95-CFP) experiments in live boutons.

Endocytosis during an ongoing 20 Hz stimulation displays a typical pattern. Four to five seconds after stimulus onset, a contingent of vesicles (Fig. 1*D*) is retrieved generating a sudden increase in total fluorescence. This finding argues for a fast recycling mechanism whereby vesicles are re-used during the first seconds of stimulation. Interestingly, the vesicle number taken up by 40 APs was independent of stimulation frequency, hinting towards one vesicle pool serving both slow and short bursts of fast exocytosis. Sara *et al.* (2002) used the discrepancy between postsynaptic current recordings and destaining to determine the time course of re-use (Sara *et al.* 2002). Similarly, they found that re-use could be measured as early as 2–3 s after stimulus onset, without however, observing a second destaining phase. Alternatively, a similar upload pattern would appear if exocytosis ceased completely to resume again after 5 s, which is unlikely. However, membrane accumulation slowed endocytosis at the calyx of Held (Sun *et al.* 2002), and clathrin recruitment to sites of endocytosis was found to be delayed by 5–10 s during prolonged 20 Hz stimulation, suggesting that early endocytosis is either clathrin independent or involves preassembled coat structures (Mueller *et al.* 2004). This may explain the upload plateau at 5 s found in our study equally well. Also Fernandez-Alfonso & Ryan (2004) showed that at room temperature there is membrane accumulation during 20 Hz stimulation and that endocytosis cannot keep up with exocytosis. It cannot be excluded that the total upload with 400 AP (20 Hz) would have been higher if the dye was left in for longer than 35 s. However, preliminary experiments (dye present for 100 s) suggest that this was not the case and also there is no reason to assume that incomplete endocytosis would alter the typical upload pattern for the shorter stimuli.

In contrast to the recent report on snake motor nerve terminals (Lin *et al.* 2005), where recently recycled vesicles independently of stimulus frequency seem to have a lower than random probability to be re-used, the destaining differences after low or high frequency loading suggest that post-endocytic trafficking depends on stimulus strength. Instead of using delayed load or immediate wash protocols (Richards *et al.* 2003), we used low and high frequency stimulation to address endocytic differences. Low frequency stimulation sorted vesicles such that they were released preferentially. Faster destaining can only occur if vesicles are not mixing randomly. Although stimuli used here are more subtle (400 instead of 1800 APs), our results are in line with findings in frog NMJ (Richards *et al.* 2000, 2003; Rizzoli & Betz, 2004). Richards *et al.* (2003) used a short stimulus ('buzz') to release RRP vesicles prior to destaining, which caused a destaining delay. In hippocampal boutons we did not observe such delay, although destaining set off slower (P. Vanden Berghe & J. Klingauf, unpublished data). This may be due to our stimulation protocol which may not perfectly distinguish between vesicle pools in these small boutons.

To provide further evidence for specialized post-endocytic routes, we developed a technique to simultaneously monitor vesicles after either stimulus. We made use of spectrally different FM dyes with similar departitioning properties for either low or high frequency

stimulation. Independently of the dye, low frequency stimulation vesicles went first during destaining, which corroborates the idea of a 'local' or 'shortcut' endocytic route conveying vesicles directly to the front of the release queue. The nature of these pathways (see review by Royle & Lagnado, 2003), 'kiss and run' or full collapse (Aravanis *et al.* 2003; Gandhi & Stevens, 2003), clathrin mediated or not (Murthy & Stevens, 1998) cannot be derived from these data. By using a 2-step protocol with different colours we were able to target two different uptake routes. If freshly endocytosed vesicles would sit in the back of the queue, then relative destaining of the second colour would be slower. If all vesicles are treated equally and randomly mix in the bouton then, relative destaining should be the same. The fact that we measure a relative faster destaining for the vesicles stained with the last step, strongly suggests that these are preferentially used. Destaining differences are rather small, which is not unexpected given the measured fractions of coloured vesicles in RRP (sucrose data, Fig. 5*B*) and resting pools (remaining fractions after high frequency destaining, Fig. 5*A*). Moreover convolution with slow dye departitioning and clearance ($\sim$5 s) and low signal to noise of fractional signals at hippocampal boutons may also explain why differences are smaller than for frog NMJ (Richards *et al.* 2003; Rizzoli & Betz, 2004). The reason why both colours are present in all pools may be that the stimuli fail to discriminate well enough between pools or alternatively due to inter- or back-mixing (Murthy & Stevens, 1999) during washing ($>$ 5 min). Yet, there is a marked difference, which, if washing times, necessary to remove excess dye, could be shortened and stimuli optimized to better select pools, might result in bigger spatial and kinetic differences. We also observed a small increase in background fluorescence remaining after 'complete' destaining of the boutons loaded with high frequency stimuli. This may indicate that some dye is still left, either in endosomes or lingering vesicles, which actually leads to an overestimation of the high frequency fraction released by 400 APs. Nevertheless, this provides evidence for co-existence of two pathways, one employed after high and one after low frequency stimulation, in which the latter sorts or tags vesicles such that they have a higher re-use probability. We also used high K^+ as a strong stimulus combined with the 2 Hz restaining protocol and measured the same effect. Vesicles loaded with the latest, low frequency stimulation were used preferentially. Fernandez-Alfonso & Ryan (2004) showed that during 2 Hz stimulation (and higher for physiological temperatures) a steady state is reached between exo- and endocytosis. At higher frequencies exo- out-competes endocytosis resulting in a net accumulation of membrane. It is not inconceivable that membrane parts are retrieved later via different mechanisms or at different sites, eventually generating spatial differences. In addition, one recycling mode might, in contrast to the other, involve endosomes as intermediates. The involvement of endosomes could actually be an attractive explanation for the observed differences. If for strong stimulation more vesicles had to be redrawn from an endosome, this would definitely result in a delayed destaining. Also it seems plausible that large structures such as endosomes are not located at or close to the active zone. Therefore the use of an endosomal intermediate could support both our kinetic and spatial observations.

Another advantage of dual colour experiments is that spatial aspects can be addressed in live hippocampal boutons. In Drosophila NMJ, Kuromi & Kidokoro (1998) determined the location of resting pool vesicles as centred, while recycling vesicles were residing at the bouton periphery. Due to the size of hippocampal boutons 'centre' and 'periphery' are hard to define. This problem can be partially overcome by determining relative positions of clusters with different colours. In control experiments we addressed putative technical pitfalls caused by, e.g. chromatic aberration, scan imprecision or signal-to-noise levels (cf. Methods and Fig. 5*F* and *G*). The imprecision for determination of the relative centre positions of the differently labelled vesicle pools was only about 25 nm, due to simultaneous recording eliminating the problem of scanning imprecision and due to the high signal-to-noise ratio obtained for ensembles of stained vesicles. Thus, the slight differences in relative position of the two vesicle pools cannot be attributed to measurement artefacts. Even for single FM-143 stained vesicles, with low signal-to-noise ratios as compared with this study, we recently could track with repetitive scanning their relative position in single boutons with a precision of about 60 nm (Lemke & Klingauf, 2005).

Neither can the differences in position or shape be explained by the discreteness of vesicle staining if a reasonable amount of vesicles were randomly mixing within the bouton. Different to an almost random organization in frog NMJ (Rizzoli & Betz, 2004), these findings argue for a specific location. Vesicles stained during low frequency stimulation generated a more circular spot, suggesting that they either stay local or follow a track leading to a confined area. This supports earlier EM findings (Schikorski & Stevens, 2001) showing RRP vesicles to correlate with those docked at the active zone. The more ellipsoidal appearance after high frequency stimulation may result from membrane retrieval at (Heuser & Reese, 1973; Rizzoli & Betz, 2004) or transport towards the active zone periphery. Whether the observed effects are due to different sorting of specific vesicles or the outcome of different endocytic routes (for review see Royle & Lagnado, 2003), involving endosomes or not, remains to be unravelled.

Besides shape and relative position, we tried to relate vesicle cluster position to structural information. From DIC images and fluorescence images of

PSD-95-CFP-tagged postsynaptic sites we could derive that the distance between the active zone and vesicle clusters labelled by low frequency stimulation was smaller than for other vesicles. This again supports the idea that the first are either endocytosed close to or conveyed back towards the active zone, corroborating ultrastructural EM data (Schikorski & Stevens, 2001). An advantage of light optical techniques over EM is that, besides being less labour intensive, vesicles can be studied in live boutons in space and time. Although Betz *et al.* (1992) did not observe changes in cluster shape during destaining of frog NMJ using one colour, multiple colour experiments may generate a more detailed view on vesicle organization within a bouton. Given the new microscopy developments to improve resolution (Hell, 2003), light microscopy may be the method of choice to study rearrangement of vesicles during exo- and endocytosis.

Figure 7*H* summarizes all our findings: high frequency stimulation vesicles (red) outnumber low frequency stimulation vesicles (green) about two-fold (cf. Figure 4*D*). They are recycled back differently into kinetically distinct pools (p1 = RRP and p3 = resting pool, cf. Figs 4*E*, and 5*A* and *B*) and a model with three sequentially arranged pools mimics all data remarkably well. The resulting centre of mass (circles) (cf. Fig. 6*F*) of vesicles endocytosed by low frequency stimulation is closer to the active zone (cf. Fig. 7*G*). What is the molecular mechanism rendering vesicles endocytosed last, kinetically and spatially privileged? Is it simply a consequence of molecularly different endocytosis pathways or are recently endocytosed vesicles destined for re-use by a memory tag (Holt & Jahn, 2004)? If so, this tag may be rather short lived as vesicles are quickly arranged spatially in hippocampal synapses. Alternatively, vesicles endocytosed last may be brought to the edge of the cluster, somewhat closer to the active zone than the centre of the vesicle cluster. This way these vesicles would be less tightly integrated into the cluster. They could be even attached to actin, which is found at the periphery (Sankaranarayanan *et al.* 2003). Those vesicles could then more easily reach the active zone than vesicles deep inside the cluster. Such a scenario would be in line with electron microscopic data by Rizzoli & Betz (2004) as pointed out by the authors and would nicely explain the prevalence of angles around 90 deg in the angular distribution of pool centre positions relative to the PSD (Fig. 7). Although debated (Wu & Betz, 1996), Ca^{2+} may be pivotal in vesicle arrangement (Kuromi & Kidokoro, 2002; Kuromi *et al.* 2004). Presynaptic $[Ca^{2+}]_i$ may differ substantially during low or high frequency stimulation, setting via Ca^{2+}/calmodulin-dependent kinases the phosphorylation level of synapsins known to tether vesicles to the cytoskeleton (Chi *et al.* 2003). The future challenge will be to identify the molecular players (Virmani *et al.* 2003) selecting and distributing vesicles over the release queue.

References

Aravanis AM, Pyle JL & Tsien RW (2003). Single synaptic vesicles fusing transiently and successively without loss of identity. *Nature* **423**, 643–647.

Betz WJ & Bewick GS (1992). Optical analysis of synaptic vesicle recycling at the frog neuromuscular junction. *Science* **255**, 200–203.

Betz WJ, Bewick GS & Ridge RM (1992). Intracellular movements of fluorescently labeled synaptic vesicles in frog motor nerve terminals during nerve stimulation. *Neuron* **9**, 805–813.

Ceccarelli B, Hurlbut WP & Mauro A (1973). Turnover of transmitter and synaptic vesicles at the frog neuromuscular junction. *J Cell Biol* **57**, 499–524.

Chi P, Greengard P & Ryan TA (2003). Synaptic vesicle mobilization is regulated by distinct synapsin I phosphorylation pathways at different frequencies. *Neuron* **38**, 69–78.

de Lange RP, de Roos AD & Borst JG (2003). Two modes of vesicle recycling in the rat calyx of Held. *J Neurosci* **23**, 10164–10173.

Fernandez-Alfonso T & Ryan TA (2004). The kinetics of synaptic vesicle pool depletion at CNS synaptic terminals. *Neuron* **41**, 943–953.

Fesce R, Grohovaz F, Valtorta F & Meldolesi J (1994). Neurotransmitter release: fusion or 'kiss-and-run'? *Trends Cell Biol* **4**, 1–4.

Gandhi SP & Stevens CF (2003). Three modes of synaptic vesicular recycling revealed by single-vesicle imaging. *Nature* **423**, 607–613.

Harata N, Pyle JL, Aravanis AM, Mozhayeva M, Kavalali ET & Tsien RW (2001). Limited numbers of recycling vesicles in small CNS nerve terminals: implications for neural signaling and vesicular cycling. *Trends Neurosci* **24**, 637–643.

Hell SW (2003). Toward fluorescence nanoscopy. *Nat Biotechnol* **21**, 1347–1355.

Heuser JE & Reese TS (1973). Evidence for recycling of synaptic vesicle membrane during transmitter release at the frog neuromuscular junction. *J Cell Biol* **57**, 315–344.

Holt M & Jahn R (2004). Neuroscience. Synaptic vesicles in the fast lane. *Science* **303**, 1986–1987.

Klingauf J, Kavalali ET & Tsien RW (1998). Kinetics and regulation of fast endocytosis at hippocampal synapses. *Nature* **394**, 581–585.

Koenig JH & Ikeda K (1996). Synaptic vesicles have two distinct recycling pathways. *J Cell Biol* **135**, 797–808.

Kuromi H, Honda A & Kidokoro Y (2004). Ca^{2+} influx through distinct routes controls exocytosis and endocytosis at Drosophila presynaptic terminals. *Neuron* **41**, 101–111.

Kuromi H & Kidokoro Y (1998). Two distinct pools of synaptic vesicles in single presynaptic boutons in a temperature-sensitive Drosophila mutant, shibire. *Neuron* **20**, 917–925.

Kuromi H & Kidokoro Y (1999). The optically determined size of exo/endo cycling vesicle pool correlates with the quantal content at the neuromuscular junction of Drosophila larvae. *J Neurosci* **19**, 1557–1565.

Kuromi H & Kidokoro Y (2002). Selective replenishment of two vesicle pools depends on the source of Ca^{2+} at the Drosophila synapse. *Neuron* **35**, 333–343.

Lemke EA & Klingauf JK (2005). Single synaptic vesicle tracking in individual hippocampal boutons at rest and during synaptic activity. *J Neurosci* **25**, 11034–11044.

Li Z, Burrone J, Tyler WJ, Hartman KN, Albeanu DF & Murthy VN (2005). Synaptic vesicle recycling studied in transgenic mice expressing synaptopHluorin. *Proc Natl Acad Sci U S A* **102**, 6131–6136.

Lin MY, Teng H & Wilkinson RS (2005). Vesicles in snake motor terminals comprise one functional pool and utilize a single recycling strategy at all stimulus frequencies. *J Physiol* **568**, 413–421.

Miller TM & Heuser JE (1984). Endocytosis of synaptic vesicle membrane at the frog neuromuscular junction. *J Cell Biol* **98**, 685–698.

Mueller VJ, Wienisch M, Nehring RB & Klingauf J (2004). Monitoring clathrin-mediated endocytosis during synaptic activity. *J Neurosci* **24**, 2004–2012.

Murthy VN & Stevens CF (1998). Synaptic vesicles retain their identity through the endocytic cycle. *Nature* **392**, 497–501.

Murthy VN & Stevens CF (1999). Reversal of synaptic vesicle docking at central synapses. *Nat Neurosci* **2**, 503–507.

Pieribone VA, Shupliakov O, Brodin L, Hilfiker-Rothenfluh S, Czernik AJ & Greengard P (1995). Distinct pools of synaptic vesicles in neurotransmitter release. *Nature* **375**, 493–497.

Pyle JL, Kavalali ET, Piedras-Renteria ES & Tsien RW (2000). Rapid reuse of readily releasable pool vesicles at hippocampal synapses. *Neuron* **28**, 221–231.

Richards DA, Guatimosim C & Betz WJ (2000). Two endocytic recycling routes selectively fill two vesicle pools in frog motor nerve terminals. *Neuron* **27**, 551–559.

Richards DA, Guatimosim C, Rizzoli SO & Betz WJ (2003). Synaptic vesicle pools at the frog neuromuscular junction. *Neuron* **39**, 529–541.

Rizzoli SO & Betz WJ (2004). The structural organization of the readily releasable pool of synaptic vesicles. *Science* **303**, 2037–2039.

Rosenmund C & Stevens CF (1996). Definition of the readily releasable pool of vesicles at hippocampal synapses. *Neuron* **16**, 1197–1207.

Royle SJ & Lagnado L (2003). Endocytosis at the synaptic terminal. *J Physiol* **553**, 345–355.

Ryan TA, Reuter H, Wendland B, Schweizer FE, Tsien RW & Smith SJ (1993). The kinetics of synaptic vesicle recycling measured at single presynaptic boutons. *Neuron* **11**, 713–724.

Sankaranarayanan S, Atluri PP & Ryan TA (2003). Actin has a molecular scaffolding, not propulsive, role in presynaptic function. *Nat Neurosci* **6**, 127–135.

Sara Y, Mozhayeva MG, Liu X & Kavalali ET (2002). Fast vesicle recycling supports neurotransmission during sustained stimulation at hippocampal synapses. *J Neurosci* **22**, 1608–1617.

Schikorski T & Stevens CF (2001). Morphological correlates of functionally defined synaptic vesicle populations. *Nat Neurosci* **4**, 391–395.

Schneggenburger R & Neher E (2000). Intracellular calcium dependence of transmitter release rates at a fast central synapse. *Nature* **406**, 889–893.

Stevens CF & Tsujimoto T (1995). Estimates for the pool size of releasable quanta at a single central synapse and for the time required to refill the pool. *Proc Natl Acad Sci U S A* **92**, 846–849.

Sudhof TC (2000). The synaptic vesicle cycle revisited. *Neuron* **28**, 317–320.

Sun JY, Wu XS & Wu LG (2002). Single and multiple vesicle fusion induce different rates of endocytosis at a central synapse. *Nature* **417**, 555–559.

Virmani T, Han W, Liu X, Sudhof TC & Kavalali ET (2003). Synaptotagmin 7 splice variants differentially regulate synaptic vesicle recycling. *EMBO J* **22**, 5347–5357.

Wu LG & Betz WJ (1996). Nerve activity but not intracellular calcium determines the time course of endocytosis at the frog neuromuscular junction. *Neuron* **17**, 769–779.

Acknowledgements

We would like to thank Dr Erwin Neher for fruitful discussions and constant support and Ruud Toonen for providing the PSD-95-eXFP plasmid DNA. We are indebted to Michael Pilot for the expert technical assistance and to the lab members for their helpful comments during this study. This work was supported by grants from the Deutsche Forschungsgemeinschaft (SFB 523) and the Human Frontier Science Program (both to J.K.), and P.V.B. is a postdoctoral fellow of the F.W.O. (Fonds voor Wetenschappelijk Onderzoek (Fund for Scientific Research)), Flanders, Belgium.

Authors present address

P. Vanden Berghe: Center for Gastroenterological Research, Lab 701, KU Leuven, 3000 Leuven, Belgium. pieter.vandenberghe@med.kuleuven.be